symmetry

MDPI

Article

A Balanced Symmetrical Branch-Line Microstrip Coupler for 5G Applications

Salah I. Yahya [1,2](iD), Farid Zubir [3,*](iD), Leila Nouri [4,5,*](iD), Fawwaz Hazzazi [6](iD), Zubaida Yusoff [7,*](iD), Muhammad Akmal Chaudhary [8](iD), Maher Assaad [8](iD), Abbas Rezaei [9](iD) and Binh Nguyen Le [4,5]

1   Department of Communication and Computer Engineering, Cihan University-Erbil, Erbil 44001, Iraq; salah.ismaeel@koyauniversity.org
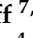2   Department of Software Engineering, Faculty of Engineering, Koya University, Koya KOY45, Iraq
3   Wireless Communication Centre, Faculty of Electrical Engineering, Universiti Teknologi Malaysia, Johor Bahru 81310, Johor, Malaysia
4   Institute of Research and Development, Duy Tan University, Da Nang 50000, Vietnam; bnlnguyen@duytan.edu.vn
5   School of Engineering & Technology, Duy Tan University, Da Nang 50000, Vietnam
6   Department of Electrical Engineering, College of Engineering in Al-Kharj, Prince Sattam bin Abdulaziz University, Al-Kharj 11492, Saudi Arabia; f.hazzazi@psau.edu.sa
7   Faculty of Engineering, Multimedia University, Persiaran Multimedia, Cyberjaya 63100, Selangor, Malaysia
8   Department of Electrical and Computer Engineering, Ajman University, Ajman P.O. Box 346, United Arab Emirates; m.akmal@ajman.ac.ae (M.A.C.); m.assaad@ajman.ac.ae (M.A.)
9   Department of Electrical Engineering, Kermanshah University of Technology, Kermanshah 67146, Iran; a.rezaee@kut.ac.ir
*   Correspondence: faridzubir@utm.my (F.Z.); leilanouri@duytan.edu.vn (L.N.); zubaida@mmu.edu.my (Z.Y.)

Abstract: Symmetry in designing a microstrip coupler is crucial because it ensures balanced power division and minimizes unwanted coupling between the coupled lines. In this paper, a filtering branch-line coupler (BLC) with a simple symmetrical microstrip structure was designed, analyzed and fabricated. Based on a mathematical design procedure, the operating frequency was set at 5.2 GHz for WLAN and 5G applications. Moreover, an optimization method was used to improve the performance of the proposed design. It occupied an area of 83.2 mm^2. Its harmonics were suppressed up to 15.5 GHz with a maximum level of −15 dB. Meanwhile, the isolation was better than −28 dB. Another advantage of this design was its high phase balance, where the phase difference between its output ports was 270° ± 0.1°. To verify the design method and simulation results, the proposed coupler was fabricated and measured. The results show that all the simulation, design methods, and experimental results are in good agreement. Therefore, the proposed design can be easily used in designing high-performance microstrip-based communication systems.

Keywords: microstrip; coupler; phase; filtering response; 5G application; coupling factor

1. Introduction

Microstrip devices play a crucial role in RF communication systems as they allow for the miniaturization, integration, and cost-effective realization of various components such as filters, couplers, power dividers, and antennas [1–4]. Since microstrip couplers have been in wide-spread demand for modern wireless communication systems, several novel types have been reported recently. Using step-impedance cells, a microstrip branch-line coupler (BLC) was designed in [5]. It operates at 2.4 GHz, which makes it suitable for wireless local area networks (WLANs). Several types of BLCs are presented in [6–8], and all of them display the common problem of phase unbalance. One of the advantages of designing a coupler is that it yields a filtering frequency response. However, in [9–13], the designers used the microstrip structures to obtain five couplers without any filtering frequency responses. Also, they could not improve the phase balance in their designs. A three-channel microstrip coupler with a filtering frequency response is reported in [14].

However, it occupies a very large implementation area without suppressing the harmonics. Two microstrip couplers are proposed in [15,16] with large sizes, high insertion loss and high coupling factor. Using the T-shaped microstrip stubs, a coupler was designed in [17] for 5G high-band applications. The presented microstrip couplers in [18,19] are suitable for Global System for Mobile Communications (GSM) applications. However, they could not attenuate the harmonics. Also, the proposed coupler in [18] is very large. In [20], a microstrip of −3 dB BLC was achieved using open-circuited coupled lines. A microstrip coupler for use in Worldwide Interoperability for Microwave Access (WiMAX) applications is reported in [21], but it does not have a filtering frequency response. A summary of the advantages, disadvantages, design methods and applications of the above-reported couplers are listed in Table 1.

Table 1. The specifications of the previous couplers.

Refs.	Advantages	Disadvantages	Design Method	Applications
[5]	Balanced phase	No filtering response	Calculation of the reflection coefficient	WLAN-5G
[6]	---	No filtering response, Phase unbalance	Analysis of the ABCD matrix of a transmission line	5G
[7]	Filtering response, Compact size	High losses	No mathematical design	GSM
[8]	Novel structure	Phase unbalance	No mathematical design	5G
[9]	---	Phase unbalance, Magnitude unbalance, No filtering response	Calculation of the line impedance and power ratio between output ports	5G
[10]	---	No filtering response, High loss, Phase unbalance, Magnitude unbalance	No mathematical design	WiMAX-5G
[12]	---	No filtering response	No mathematical design	5G
[13]	Low losses	No filtering response, Phase unbalance	Calculation of the input impedance of the basic resonator	WLAN-5G
[16]	Filtering response, Novel structure	Large size, Phase unbalance	Obtaining the output-input voltage ratio	5G

In this work, we present a microstrip BLC with a novel structure. It has a filtering frequency response, which can suppress the 1st and 2nd harmonics up to 15.5 GHz. Operating at 5.2 GHz makes it suitable for IEEE 802.11a WLAN and mid-band 5G applications. A lowpass resonator is proposed and mathematically analyzed to use in the coupler structure. The proposed coupler is obtained through the direct integration of two lowpass filters (LPFs) and we did not change the dimensions of the LPFs in the final coupler structure. However, the additional optimization is performed to improve its performance. Our design has a high performance, and it can be easily integrated with the other high frequency circuits for designing RF communication systems.

The final layout of the designed coupler is optimized to improve its performance. Good insertion loss, isolation, phase balance and coupling factor are obtained, while the return loss and the coupler size (83.2 mm^2) are acceptable. This manuscript is organized as follows. Section 1 provides the introduction. Section 2 provides the presented mathematical analysis and optimization of the proposed resonator, filters and coupler. Section 3 presents

the simulation and measurement results, description of the measurements setup and comparison with the previous works. Finally, Section 4 concludes the paper.

2. Design of Resonator, Filters and Coupler

Figure 1 shows a symmetrical stub-loaded transmission line with its equivalent LC circuit. The stub is a low-impedance cell. The lines with the physical lengths l_a and l_b are replaced by the inductors L_a and L_b, respectively. Also, the open end of the shunt stub is presented by the C_o capacitor.
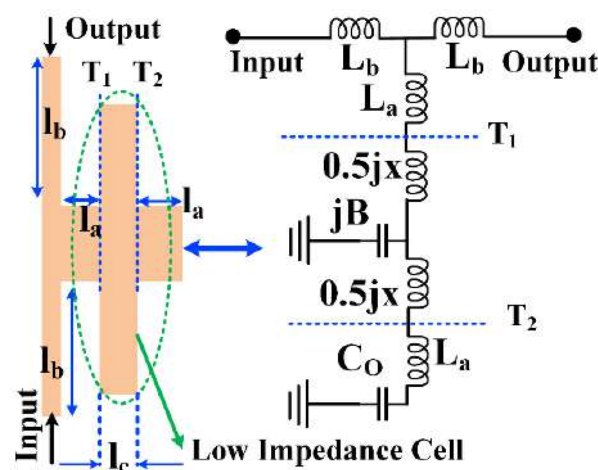

Figure 1. Layout and LC circuit of the proposed resonator.

The equivalent circuit from T_1 to T_2 is presented by two inductors with two equivalent impedances of 0.5jx and a capacitor with an equivalent impedance of jB. For a short-line l_c ($l_c < (\lambda_g/8)$) with a characteristic impedance of Z_c, the values of x and B can be approximated by [22]:

$$x \approx Z_c\left(\frac{2\pi\, l_c}{\lambda_g}\right) \ \& \ B \approx \frac{1}{Z_c}\left(\frac{2\pi\, l_c}{\lambda_g}\right) \tag{1}$$

where λ_g and l_c are the guided wavelength and the physical length from T_1 to T_2, respectively. The equivalent impedance of the shunt stub (Z_{Sh}) can be calculated as follows:

$$Z_{Sh} = \frac{1}{\left(\frac{1}{\frac{1}{j\omega C_o}+j\omega(L_a+0.5x)}\right)+j\omega B} + j\omega(L_a+0.5x) \Rightarrow$$

$$Z_{Sh} = \frac{1-\omega^2 C_o(L_a+0.5x)+j\omega(L_a+0.5x)[j\omega C_o+j\omega B(1-\omega^2 C_o(L_a+0.5x))]}{[j\omega C_o+j\omega B(1-\omega^2 C_o(L_a+0.5x))]} \tag{2}$$

where ω is an angular frequency and L_a and C_o are defined before and presented in Figure 1. Substituting Equation (1) into Equation (2) results in:

$$Z_{Sh} = \frac{1-\omega^2 C_o(L_a+Z_c(\frac{\pi l_c}{\lambda_g}))+j\omega(L_a+Z_c(\frac{\pi l_c}{\lambda_g}))[j\omega C_o+j\omega(\frac{2\pi l_c}{Z_c\lambda_g})(1-\omega^2 C_o(L_a+Z_c(\frac{\pi l_c}{\lambda_g})))]}{j\omega C_o+j\omega(\frac{2\pi l_c}{Z_c\lambda_g})(1-\omega^2 C_o(L_a+Z_c(\frac{\pi l_c}{\lambda_g})))} \tag{3}$$

The ABCD matrix of the proposed resonator (T_R) can be obtained through [23]:

$$T_R = \begin{bmatrix} A_R & B_R \\ C_R & D_R \end{bmatrix} = \begin{bmatrix} 1 & j\omega L_b \\ 0 & 1 \end{bmatrix} \times \begin{bmatrix} 1 & 0 \\ \frac{1}{Z_{Sh}} & 1 \end{bmatrix} \times \begin{bmatrix} 1 & j\omega L_b \\ 0 & 1 \end{bmatrix} = \begin{bmatrix} 1+\frac{j\omega L_b}{Z_{Sh}} & j\omega L_b(2+\frac{j\omega L_b}{Z_{Sh}}) \\ \frac{1}{Z_{Sh}} & 1+\frac{j\omega L_b}{Z_{Sh}} \end{bmatrix} \tag{4}$$

Using the calculated T_R, we can obtain the scattering matrix of the proposed resonator (S_R) as follows:

$$S_R = \begin{bmatrix} S_{11} & S_{12} \\ S_{21} & S_{22} \end{bmatrix} = \begin{bmatrix} \dfrac{A_R+B_R/Z_0-C_RZ_0-D_R}{A_R+B_R/Z_0+C_RZ_0+D_R} & \dfrac{2(A_RD_R-B_RC_R)}{A_R+B_R/Z_0+C_RZ_0+D_R} \\ \\ \dfrac{2}{A_R+B_R/Z_0+C_RZ_0+D_R} & \dfrac{-A_R+B_R/Z_0-C_RZ_0+D_R}{A_R+B_R/Z_0+C_RZ_0+D_R} \end{bmatrix} \Rightarrow$$

$$S_{11} = S_{22} = \frac{\frac{j\omega L_b}{Z_0}\left(2+\frac{j\omega L_b}{Z_{Sh}}\right)-\frac{Z_0}{Z_{Sh}}}{2+\frac{2j\omega L_b+Z_0}{Z_{Sh}}+\frac{j\omega L_b}{Z_0}\left(2+\frac{j\omega L_b}{Z_{Sh}}\right)}$$

$$S_{12} = S_{21} = \frac{2}{2+\frac{2j\omega L_b+Z_0}{Z_{Sh}}+\frac{j\omega L_b}{Z_0}\left(2+\frac{j\omega L_b}{Z_{Sh}}\right)}$$

(5)

In Equation (5), Z_0 is the impedance of the terminals and A_R, B_R, C_R and D_R are the transfer parameters. Also, S_{11}, S_{21}, S_{12} and S_{22} are the scattering parameters. According to Equation (3) and for low frequencies, Z_{Sh} will be an open circuit. Therefore, S_{11} and S_{21} at low frequencies will be changed as follows:

$$S_{11} = \frac{j\omega_{low}L_b}{Z_0+j\omega_{low}L_b}$$
$$S_{21} = \frac{Z_0}{Z_0+j\omega_{low}L_b}$$

(6)

where ω_{low} is a low angular frequency. From Equation (6), it is clear that the -3 dB cut-off frequency depends on the values of L_b so that a cut-off angular frequency (ω_c) can be obtained using the following equation:

$$\begin{cases} \frac{1}{\sqrt{2}}|S_{21}|_{Max} = |S_{21}| \\ |S_{21}| = \frac{Z_0}{\sqrt{2Z_0^2+2(\omega_cL_b)^2}} \\ \frac{1}{\sqrt{2}}|S_{21}|_{Max} = \frac{1}{\sqrt{2}}\left|\frac{Z_0}{Z_0+j\omega_cL_b}\right|_{Max} = \frac{Z_0}{\left\{\sqrt{2Z_0^2+2(\omega_cL_b)^2}\right\}_{Min}} = \frac{1}{\sqrt{2}} \end{cases} \Rightarrow$$

$$\frac{Z_0^2}{2Z_0^2+2(\omega_cL_b)^2} = \frac{1}{2} \Rightarrow \omega_cL_b \approx 0$$

(7)

Our target is to obtain a cut-off frequency in GHz; therefore, by choosing a L_b of less than 1 nH, ω_cL_b will be near zero. Since the simulation results show that at the cut-off frequency $|S_{21}| = |S_{11}|$, the second way to obtain the cut-off frequency is as follows:

$$|S_{21}| = |S_{11}| \Rightarrow \frac{Z_0}{\sqrt{2Z_0^2+2(\omega_cL_b)^2}} = \frac{\omega_cL_b}{\sqrt{Z_0^2+(\omega_cL_b)^2}} \Rightarrow \omega_c = \frac{Z_0}{\sqrt{2}L_b}$$

(8)

According to the cut-off angular frequency and based on Equation (8), the value of L_b can be calculated. Then, using Richards' transformation, the value of the physical length l_b can be determined. Using the analyzed lowpass resonator, two lowpass filters (LPF1, LPF2) are proposed. These LPFs with their frequency responses are depicted in Figure 2, where all dimensions are in mm. As shown in Figure 2, the cut-off frequencies of LPF1 and LPF2 are close to each other. The LPF1 has the best insertion and return losses of 0.03 dB and 24.9 dB in its passband. To design the LPF2, two shunt stubs were used. LPF2 has the best insertion and return losses of 0.006 dB and 32.7 dB in its passband. All simulation results in this work were obtained using the EM simulator of ADS software. The used substrate was a Rogers RT/duroid 5880 with h = 0.7874 mm, ε_r = 2.22 and tan (δ) = 0.0009.

To obtain a microstrip BLC, we integrated the proposed LPFs. The layout configuration of our coupler is illustrated in Figure 3, where all dimensions are in mm, and we did not change the dimensions of the LPFs in it. Also, another internal shunt stub was added near the isolation port (Port 4), which is able to improve the isolation and shift the operating frequency

simultaneously. The overall size of this coupler is 6.4 mm × 13 mm = 0.14 λ_g × 0.29 λ_g, where λ_g is the guided wavelength calculated at the operating frequency.
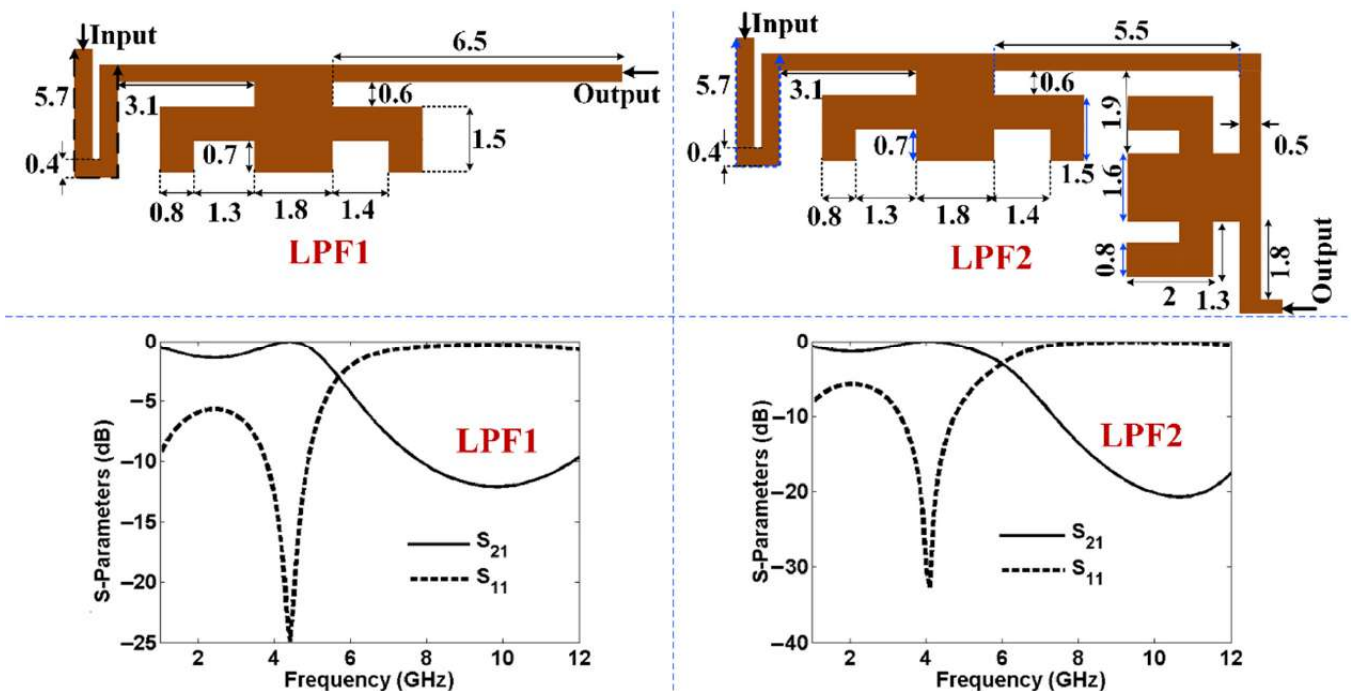

Figure 2. Layout of the proposed LPFs with their frequency responses.

Using the current density distribution, the dimensions of the physical lengths and widths l_1, l_2, w_1, w_2, w_3 and w_4 were optimized to improve the coupler performance. The current density distributions of our BLC at the operating frequency for simulating Ports 2 and 3 are shown in Figure 4. As can be seen, the thinner cells with higher impedances have higher current densities than the internal stubs. This is verified through the mathematical analysis of the proposed lowpass resonator. When we simulate Port 2 and Port 3, the upper and lower transmission lines have higher current densities, respectively. On the other hand, the upper and lower shunt stubs have higher current densities when simulating Port 2 and Port 3, respectively.
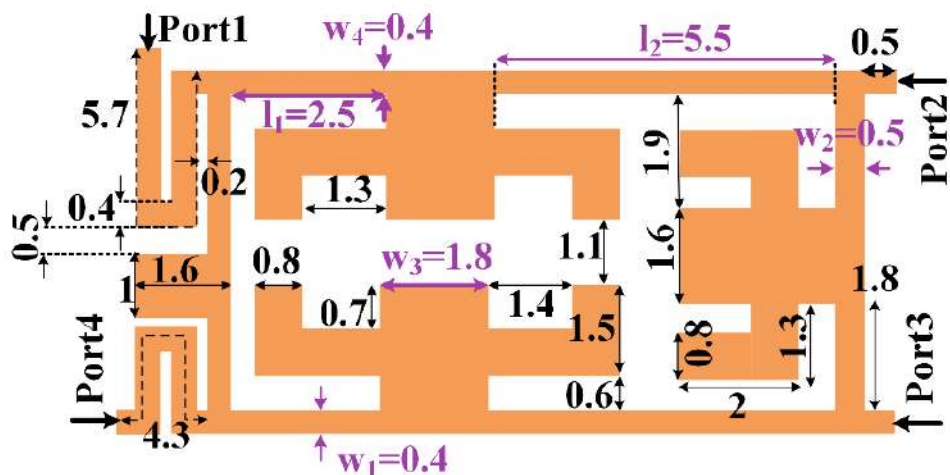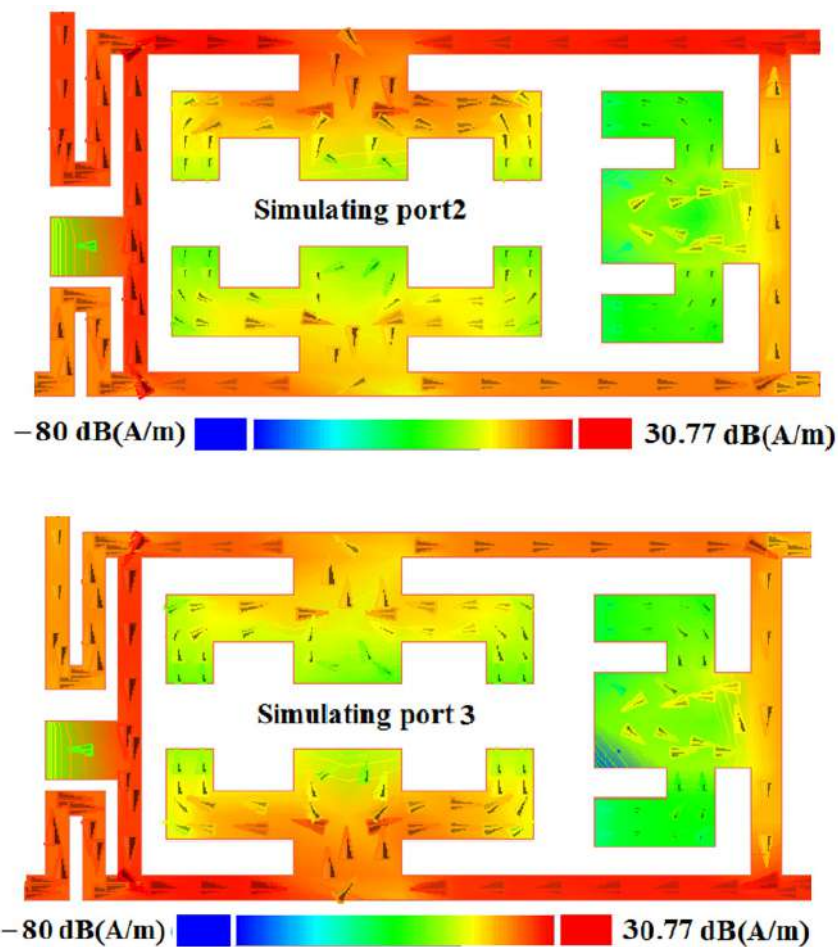

Figure 3. The proposed coupler.

Figure 4. Current density distribution of the proposed coupler at 5.2 GHz.

To improve the performance, the frequency response of the proposed coupler was obtained as functions of l_1, l_2, w_1, w_2, w_3 and w_4, and the results are presented in Figures 5 and 6. As can be seen, by increasing l_1 and l_2, the operating frequency moves to the left which verifies Equation (8). However, increasing l_1 and l_2 can improve the common port return loss (S_{11}) and isolation factor (S_{41}), which is shown in Figure 6. Decreasing the width w_1 reduces the magnitude balance of S_{21} and S_{31} but improves the return loss and isolation. On the other hand, by tuning w_3, we can increase the magnitude balance. By changing w_3, the operating frequency changes slightly. But by decreasing w_3, the isolation will be increased. By increasing w_4, the insertion loss, coupling factor (S_{31}) and isolation will be improved. However, the best value of return loss is obtained for w_4 = 0.4 mm. Figure 7 depicts the steps of our coupler design.

A phase shift of 270° will be created according to the position of the output ports in the branch line layout as well as the overall structure of the designed coupler. Thus, by tuning the physical lengths and widths of our LPFs and by changing their positions in the branch-line structure we were able to obtain a phase shift of 270° between S_{31} and S_{21}. For example, the relatively symmetrical branch line coupler with an even number of shunt stubs can create a 270° (or 90°) phase difference between the output ports. On the other hand, where the best isolation and return loss values are close to the operating frequency, the phase is balanced easily.
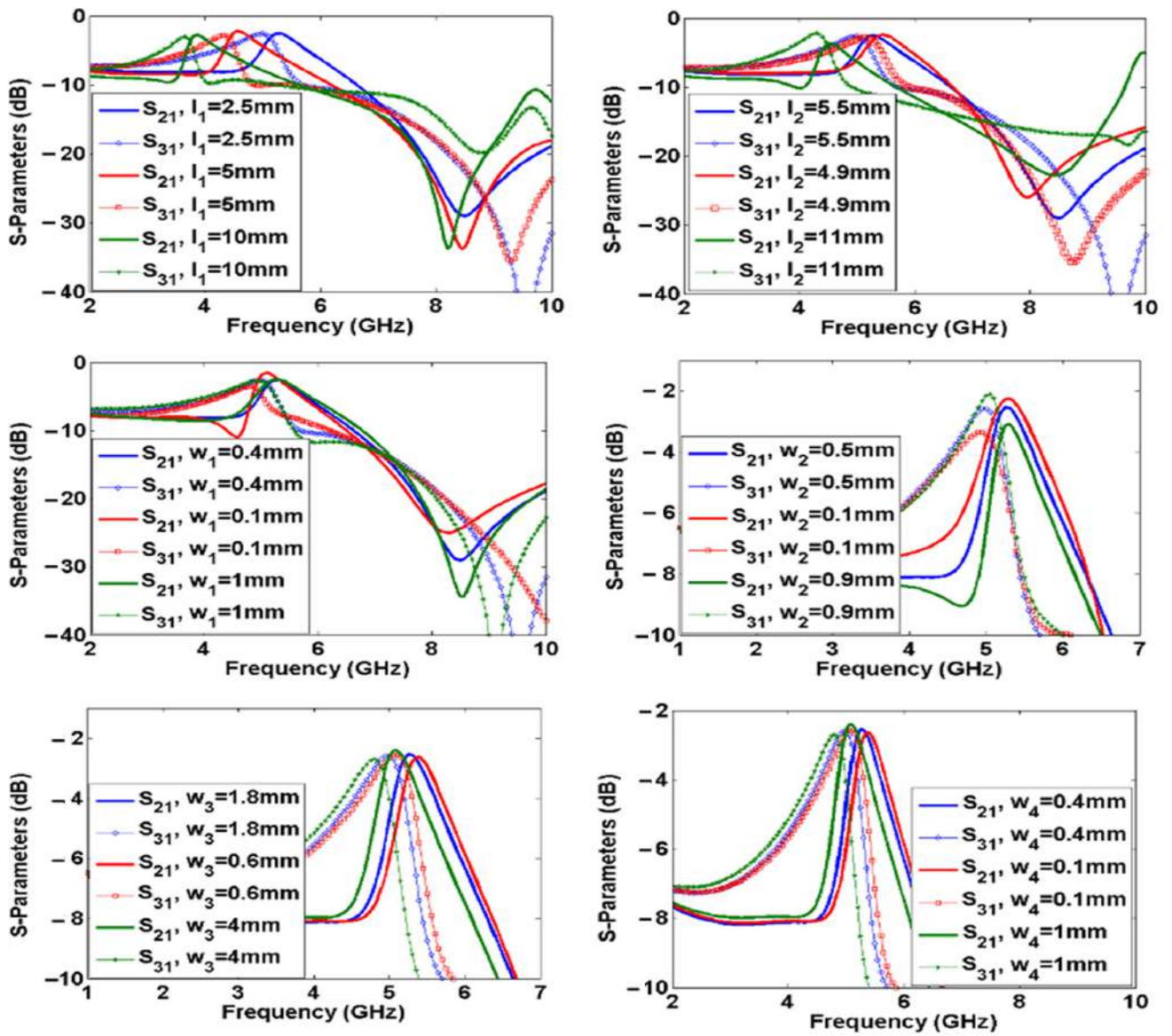
Figure 5. S_{21} and S_{31} as functions of the significant lengths and widths.
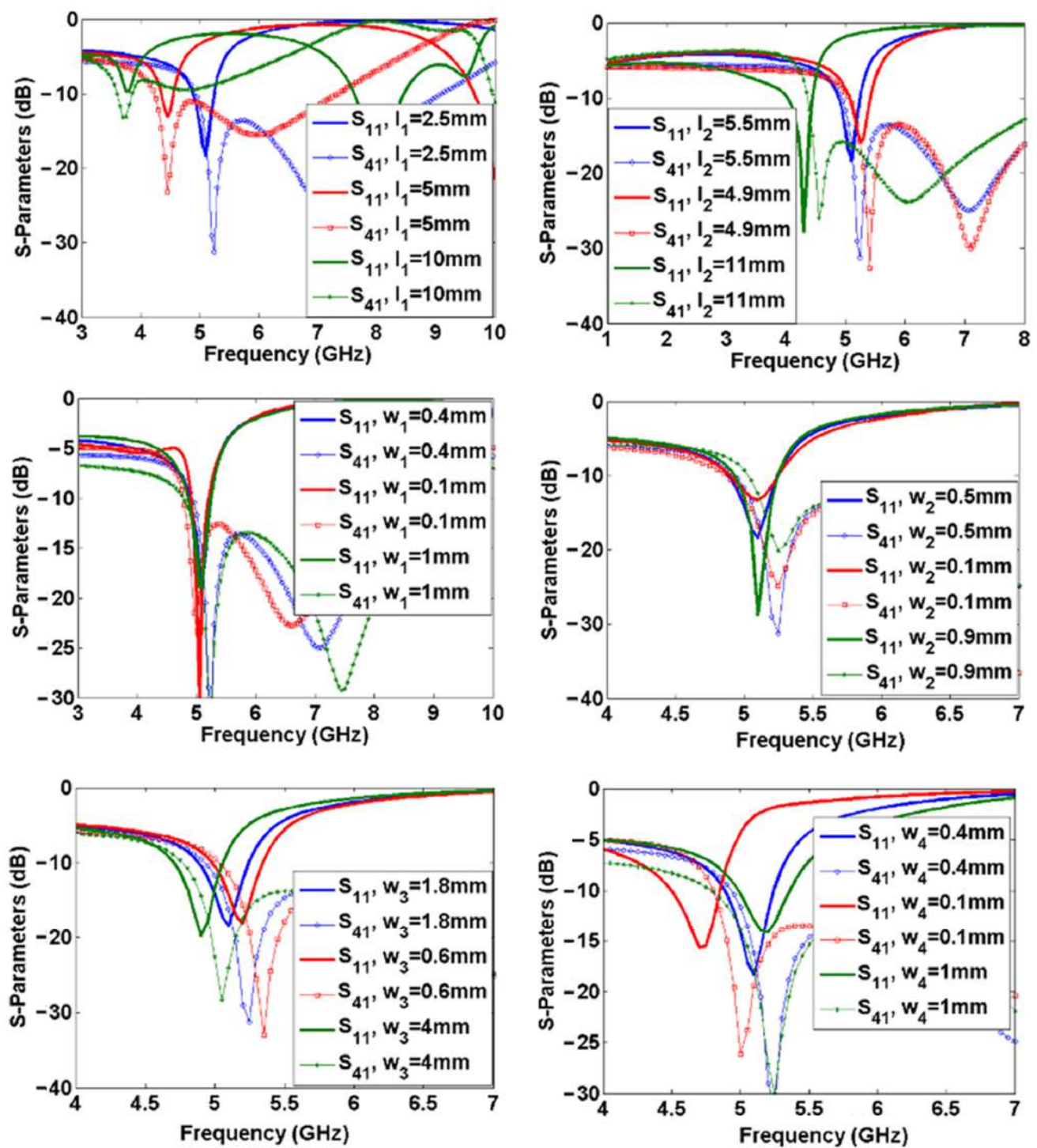
Figure 6. S_{11} and S_{41} as functions of the significant lengths and widths.
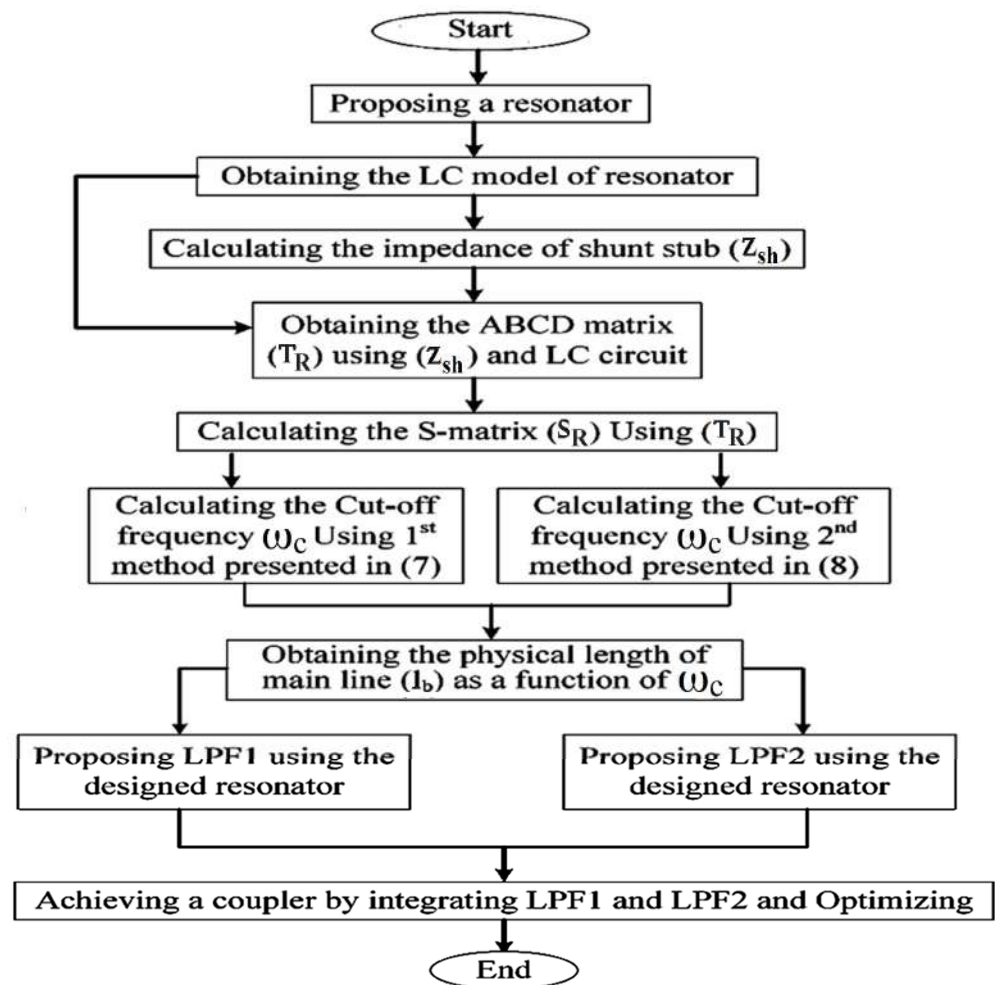
Figure 7. The steps of our coupler design.

3. Results and Comparison

We obtained the simulation results by using ADS software and the measurements were performed using an HP8757A vector network analyzer. To conduct S-parameter measurements of a branch-line coupler using a vector network analyzer (VNA), the VNA was calibrated. This process was in line with a set of calibration standards that match the frequency range and impedance of the device under test (DUT). Common standards include open, short and load terminations, as well as through-and-line standards. Using the same standards, a full two-port calibration of the VNA was performed to compensate for any systematic errors in the measurement system, such as mismatch and transmission line effects. The VNA was then configured to perform S-parameter measurements in the appropriate frequency range and measurement format, for example, the phase and magnitude or real and imaginary components, as well as the number of points and frequency step sizes for the measurements. The BLC, which is the DUT, is then connected to the RF ports of the VNA with proper coaxial connections. To measure the return loss of the BLC, Port 1 of the BLC is connected to Port 1 of the VNA, while all the other ports are terminated with 50 ohm terminators. For the BLC insertion loss measurement, Port 1 of the VNA was connected to Port 1 of the BLC, and Port 2 of the VNA was connected to Port 2 of the BLC. Port 3 and Port 4 of the BLC were terminated through the 50 ohm terminators.

Similarly, for the measurement of the BLC coupling loss, Port 1 of the VNA was connected to Port 1 of the BLC, and Port 2 of the VNA was connected to Port 3 of the BLC with Port 2 and Port 4 all terminated through 50 ohm terminators. Finally, for the measurement of the BLC's isolation loss, Port 1 of the VNA was connected to Port 1 of the BLC, and Port 2 of the VNA was connected to Port 4 of the BLC. Port 2 and Port 3 of

the BLC were terminated with 50 ohm terminators. Due to the SMA and copper losses, the simulated losses are a little better than the measurements losses. The simulated and measured frequency responses are presented in Figure 8, while Figure 9 shows the simulated and measured phase difference between S_{21} and S_{31}. The scattering parameters of proposed coupler at 5.1–5.3 GHz are depicted in Figure 10. Since the proposed structure is simple, the manufacturer error is minimal, which is an advantage. The proposed coupler works at 5.2 GHz (exactly at 5.19 GHz), which makes it suitable for WLAN and mid-band 5G (which covers 1 GHz to 6 GHz). At this operating frequency, the phase difference between S_{21} and S_{31} is $270° \pm 0.1°$. As shown in Figure 8, near the operating frequency, the best values of S_{11}, and S_{41} (isolation) are -19.6 dB and -28.2 dB, respectively. Also, the best values of S_{21} and S_{31} near the operating frequency are -2.6 dB and -2.4 dB, respectively, which are at two different frequencies. Meanwhile, at the operating frequency S_{21} and S_{31} are -3.28 dB and 3.56 dB, respectively. The harmonics are suppressed by up to 15.5 GHz with a maximum level of -15 dB. Narrowband frequency responses of the proposed coupler are shown in Figure 10. Figure 11 shows the fabricated coupler.
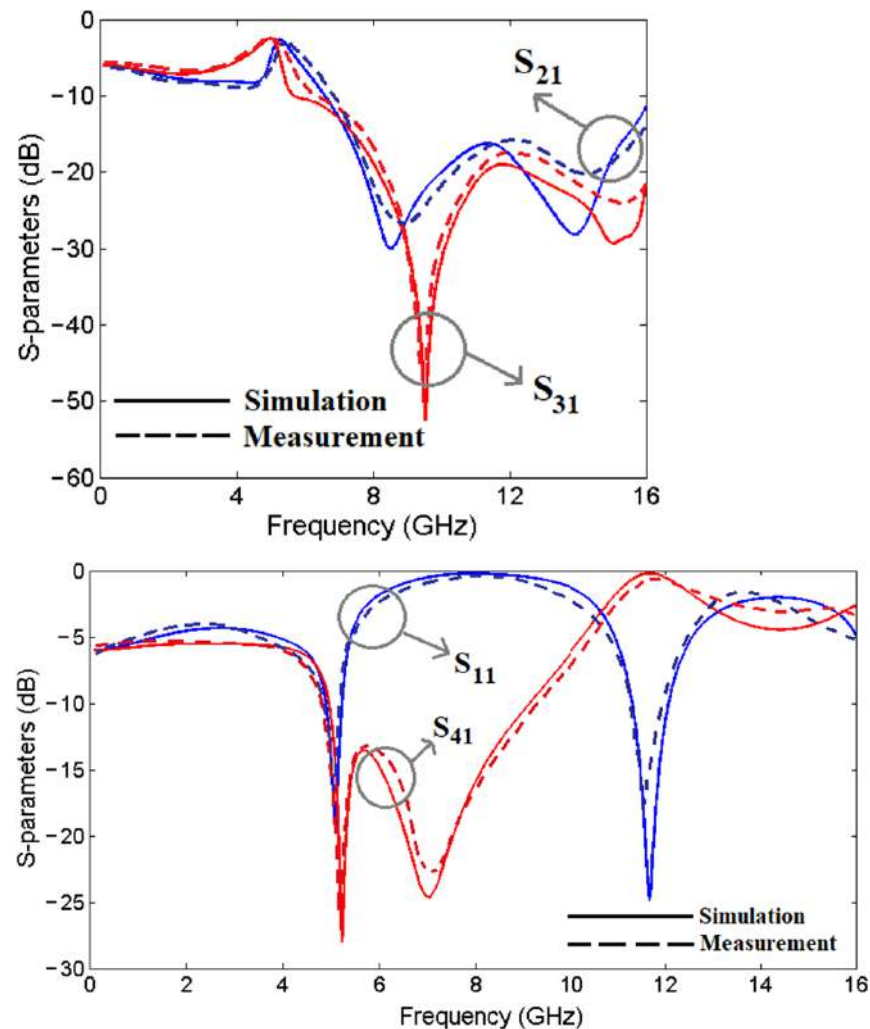

Figure 8. Simulated and measured frequency responses i.e. S_{11}, S_{21} (blue lines) and S_{41}, S_{31} (red lines).
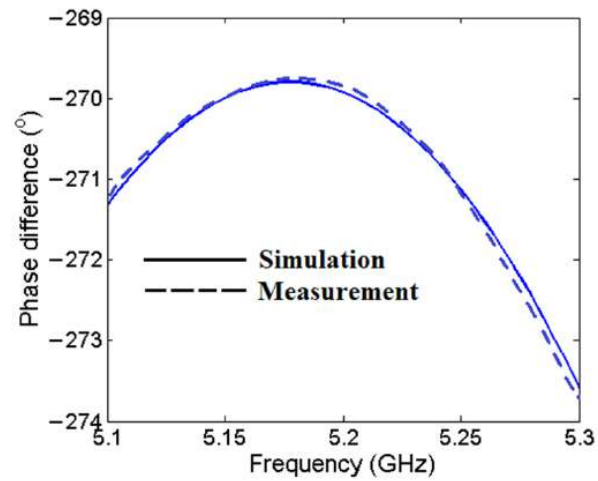
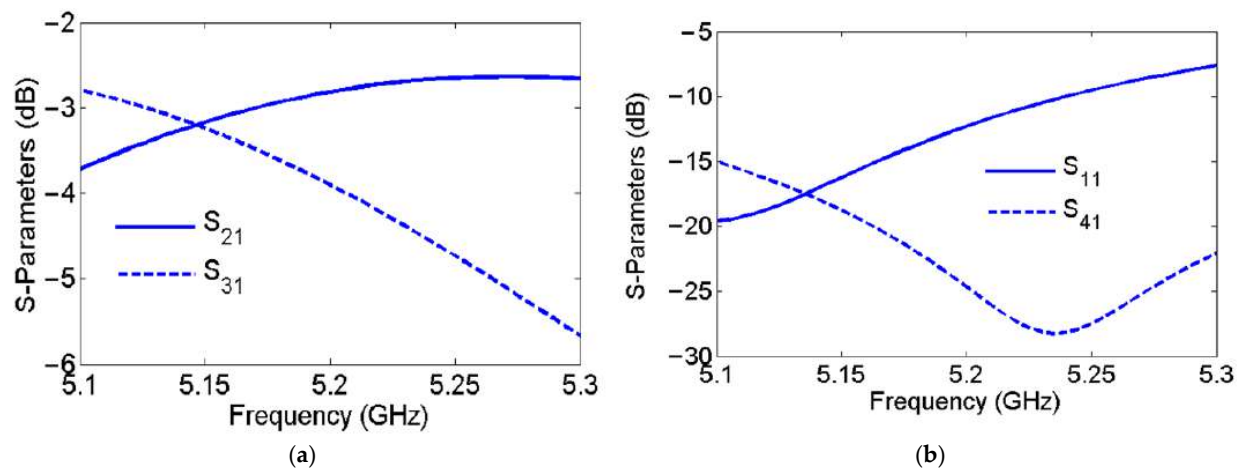**Figure 9.** Simulated and measured phase difference between S_{21} and S_{31}.

Figure 10. Narrowband frequency responses of the proposed coupler: (**a**) S_{21} and S_{31}; (**b**) S_{11} and S_{41}.
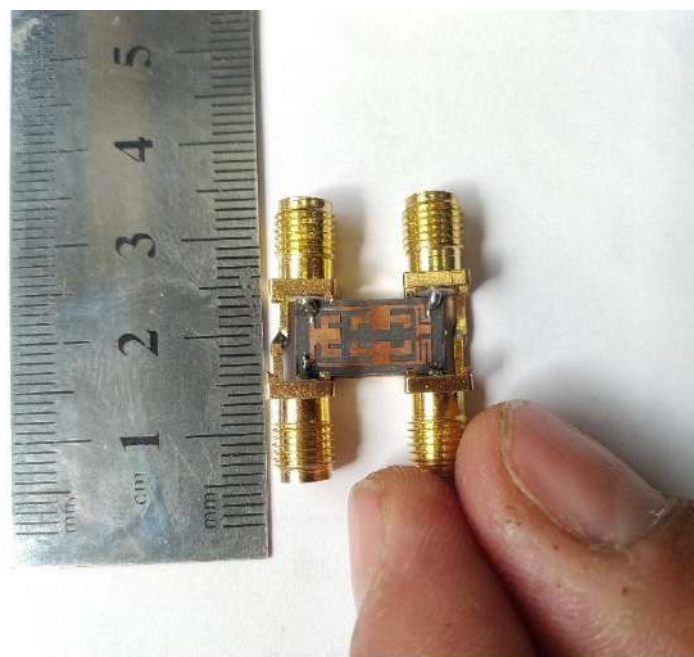

Figure 11. Fabricated Coupler.

To prove the high performance of the proposed coupler, we compared it with previous works. The comparison results are summarized in Table 2. The operating frequency, filtering response, the last frequency with suppressed harmonics and the phase unbalance are depicted by f_o, FR, LFSH and PU, respectively. As can be seen, the majority of previously reported couplers did not have a filtering frequency response and subsequently could not suppress the harmonics. Only the phase balances in [5,19,21] are a little better than ours. However, we were able to better suppress the harmonics. Moreover, the proposed designs in [5,19,21] do not have filtering frequency responses. There are four smaller couplers in Table 2 compared to ours. However, they could not suppress the harmonics well. At the operating frequency, the values of S_{21} and S_{31} are -3.28 dB and -3.56 dB. Therefore, there is a ± 0.28 dB amplitude unbalance, which is considered acceptable, since it does not have a significant negative impact on the performance.

As shown in Table 2, the isolation factor (S_{41}) near the operating frequency of this work is acceptable. The presented couplers in [5,11,19,21] were not able to suppress the harmonics, as they do not have a filtering frequency response, while our coupler suppresses harmonics of up to 15.5 GHz. The size of the proposed coupler in [16] is larger than ours. Also, our design has a better balanced amplitude and phase than the designed coupler in [16].

Table 2. Comparison with the previous works (f_o: operating frequency; FR: filtering response; LFSH: last frequency with suppressed harmonics; PU: phase unbalance; *: approximated value; **: triple-band coupler).

Refs	f_o (GHz)	FR	LFSH (GHz)	S_{21} (dB)	S_{31} (dB)	PU (Degree)	S_{41} (dB)	Size (mm^2/λ_g^2)
Our coupler	5.2	Yes	15.5	-3.28	-3.56	0.1	28.2	83.2/0.04
[5]	2.4	No	No	-3.3	-3.3	0.09	42.9	175.1/0.023
[6]	2	No	No	-3.1	-3.4	3	26 *	1322/---
[7]	0.93	Yes	1.3 *	-3.5	-3.5	---	Better than 20	673/0.017
[8]	2	Yes	4.5 *	-3.11	-3.39	1	---	265.69/---
[9]	2.9–4.1	No	No	-5	-3 ± 1	10	21 *	1524.24/---
[10]	3	No	No	-7.38	-2.25	2.3	21.5	819/---
[11]	6.3	No	No	-4.07	-4.39	2.1	30 *	2218/---
[12]	1.07	No	No	-3.3	-3.3	1	24.2	204.9/---
[13]	5.7	No	No	-2.3	-2.6	0.8	19.4	110/0.042
[14]	2.17 **	Yes	No	---	---	5	15	---/0.448
[15]	20–28.7	No	No	-3 ± 1	-3 ± 0.8	3	15 *	595/0.307 *
[16]	2.8	Yes	7	-3.3	-2.9	0.97	31.3	710/0.075
[17]	3.5	No	No	-2.97	-3.65	3.6	24.46	493/0.049
[18]	1.87	Yes	No	---	---	3	Better than 20	---/0.138
[19]	1.8	No	No	-2.9	-3.2	0.01	40	192.7/0.011
[20]	---	Yes	No	-3.6 ± 0.5	-3.6 ± 0.5	---	Better than 20	1157.5/0.2379 *
[21]	2.4	No	No	-3	-3.08	0.037	30	354.75/0.037

4. Conclusions

In this paper, we designed a symmetrical microstrip coupler using a new structure and good performance for 5G applications. It displays a filtering frequency response with suppressed harmonics, while a large number of the previous works did not cover this issue. The design method is based on analyzing a lowpass resonator to calculate the scattering parameters and find the cut-off frequency. Based on changing the significant lengths and width, the final layout structure is optimized. The simulation results extracted from the optimization method verify the presented mathematical formulas. Using the analyzed resonator, two lowpass filters are designed to be embedded in the final layout of the

proposed coupler. Finally, we compared our coupler with previous works. The comparison results showed that we were able to obtain a high phase balance and good S_{21} and S_{31} without a significant increase in the coupler size.

References

1. Jameel, M.S.; Mezaal, Y.S.; Atilla, D.C. Miniaturized Coplanar Waveguide-Fed UWB Antenna for Wireless Applications. *Symmetry* **2023**, *15*, 633. [CrossRef]
2. Wang, Z.; You, W.; Yang, M.; Nie, W.; Mu, W. Design of MIMO Antenna with Double L-Shaped Structure for 5G NR. *Symmetry* **2023**, *15*, 579. [CrossRef]
3. Roshani, S.; Yahya, S.I.; Rastad, J.; Mezaal, Y.S.; Liu, L.W.Y.; Roshani, S. Design of a Filtering Power Divider with Simple Symmetric Structure Using Stubs. *Symmetry* **2022**, *14*, 1973. [CrossRef]
4. Jamshidi, M.; Yahya, S.I.; Nouri, L.; Hashemi-Dezaki, H.; Rezaei, A.; Chaudhary, M.A. A High-Efficiency Diplexer for Sustainable 5G-Enabled IoT in Metaverse Transportation System and Smart Grids. *Symmetry* **2023**, *15*, 821. [CrossRef]
5. Salehi, M.; Noori, L. Novel 2.4 GHz branch-line coupler using microstrip cells. *Microw. Opt. Technol. Lett.* **2014**, *56*, 2110–2113. [CrossRef]
6. Chun, Y.; Hong, J. Compact Wide-Band Branch-Line Hybrids. *IEEE Trans. Microw. Theory Tech.* **2006**, *54*, 704–709. [CrossRef]
7. Hazeri, A.; Kashaninia, A.; Faraji, T.; Firouzi, M. Miniaturization and Harmonic Suppression of the Branch-Line Coupler Based on Radial Stubs. *IEICE Electron. Express* **2011**, *8*, 736–741. [CrossRef]
8. Wang, J.; Wang, B.; Guo, Y.; Ong, L.; Xiao, S. A Compact Slow-Wave Microstrip Branch-Line Coupler with High Performance. *IEEE Microw. Wirel. Comp. Lett.* **2007**, *17*, 501–503. [CrossRef]
9. Shukor, N.A.M.; Seman, N. Enhanced Design of Two-Section Microstrip-Slot Branch Line Coupler with the Overlapped k/4 Open Circuited Lines at Ports. *Springer Wirel. Pers. Commun.* **2016**, *88*, 467–488. [CrossRef]
10. Santiko, A.B.; Saputera, Y.P.; Wahyu, Y. Design and Implementation of Three Branch Line Coupler at 3.0 GHz Frequency for S-Band Radar System. In Proceedings of the 22nd Asia-Pacific Conference on Communications (APCC), Yogyakarta, Indonesia, 25–27 August 2016; pp. 315–318.
11. Velan, S.; Kanagasabai, M. Compact Microstrip Branch-Line Coupler with Wideband Quadrture Phase Balance. *Microw. Opt. Technol. Lett.* **2016**, *58*, 1369–1374. [CrossRef]
12. Shamsinejad, S.; Soleimani, M.; Komjani, N. Novel Enhanced and Miniaturized 90° Coupler for 3G EH Mixers. *IEEE Microw. Millim. Wave Technol.* **2008**, *3*, 264–1267.
13. Salehi, M.R.; Noori, L.; Abiri, E. Novel tunable branch-line coupler for WLAN applications. *Microw. Opt. Technol. Lett.* **2015**, *57*, 1081–1084. [CrossRef]
14. Liou, C.Y.; Wu, M.S.; Yeh, J.C.; Chueh, Y.Z.; Mao, S.G. A Novel Triple-Band Microstrip Branch-Line Coupler with Arbitrary Operating Frequencies. *IEEE Microw. Wirel. Compon. Lett.* **2009**, *19*, 683–685. [CrossRef]
15. Shukor, N.A.M.; Seman, N. 5G planar branch line coupler design based on the analysis of dielectric constant, loss tangent and quality factor at high frequency. *Nat. Sci. Rep.* **2020**, *10*, 16115.
16. Rezaei, A.; Noori, L. Microstrip Hybrid Coupler with a Wide Stop-Band Using Symmetric Structure for Wireless Applications. *J. Microw. Optoelectron. Electromagn. Appl.* **2018**, *17*, 23–31. [CrossRef]
17. Abdulbari, A.A.; Rahim, S.K.A.; Aziz, M.Z.A.A.; Tan, K.G.; Noordin, N.K.; Nor, M.Z.M. New design of wideband microstrip branch line coupler using T-shape and open stub for 5G application. *Int. J. Electr. Comput. Eng.* **2021**, *11*, 1346–1355. [CrossRef]
18. Shi, J.; Qiang, J.; Xu, K.; Wang, Z.b.; Lin, L.; Chen, J.X.; Liu, W.; Zhang, X.Y. A Balanced Filtering Branch-Line Coupler. *IEEE Microw. Wirel. Compon. Lett.* **2016**, *26*, 119–121. [CrossRef]

19. Nouri, L.; Yahya, S.I.; Rezaei, A. Design and Fabrication of a Compact Branch-Line Hybrid Coupler with a Balanced Phase Using a New Microstrip Structure for GSM Applications. *AEU-Int. J. Electron. Commun.* **2023**, *161*, 154529. [CrossRef]
20. Arriola, W.A.; Lee, J.Y.; Kim, I.S. Wideband 3 dB Branch Line Coupler Based on λ/4 Open Circuited Coupled Lines. *IEEE Microw. Wirel. Compon. Lett.* **2011**, *21*, 486–488. [CrossRef]
21. Rezaei, A.; Noori, L.; Hosseini, S.M. Novel microstrip branch-line coupler with low phase shift for WLANs. *Analog. Integr. Circuits Signal Process.* **2019**, *98*, 377–383. [CrossRef]
22. Hong, J.S.; Lancaster, M.J. *Microstrip Filters for RF/Microwave Applications*; John Wiley & Sons: Hoboken, NJ, USA, 2001.
23. Rezaei, A.; Yahya, S.I. A New Design Approach for a Compact Microstrip Diplexer with Good Passband Characteristics. *ARO-Sci. J. Koya Univ.* **2022**, *10*, 1–6. [CrossRef]